ACTIVE ROBUST CONTROL OF A SMART PLATE

I. Ursu[1], L. Iorga[2], A. Toader[1] and G. Tecuceanu[1]
[1]*INCAS – Elie Carafoli National Institute for Aerospace Research, Bd. Iuliu Maniu 220, 061126, Bucharest, Romania*

[2] *Now at Airbus, U.K.*

Keywords: Mechatronic Systems, Piezoelectric Smart Structures, Smart Plate, Active Vibration Control, Robust Control, H_∞ Control, LQG/LTR control, Mathematical Modeling, Laboratory Tests.

Abstract: This paper presents the development of robust controllers for piezoelectric actuated plates, in the well known framework of Riccati equations. The treatment of the modeling uncertainties is based on two approaches: robust H_∞ synthesis and LQG/LTR synthesis. The basic laboratory architecture for control laws validation is presented, with a cantilevered plate equipped with MFC actuators and strain gage sensors serving as paradigm of the smart structures. The experimental results are finally shown to testify the effect of the active control.

1 INTRODUCTION

Robust control, founded in the 1980's, focuses on the development of controllers that can maintain good performance while parameters of controlled plants incur bounded deviations. Many robust control schemes have been applied to the active control of vibration and noise, as well as smart structural systems. Yoshi and Kelkar (1998) combined LQG type synthesis with robustness and performance analysis to design a vibration controller for flexible aeroelastic modes of the supersonic aircraft. H_∞ control for vibration suppression of a plate was used by Kar *et al*., (2000) and Yaman *et al.*, (2002), where the first three modes were considered in the model and the remaining modes were treated as uncertainty. The present paper continues the previous works of the authors (I. Ursu and F. Ursu, 2002); Iorga *et al.* 2008, 2009), aiming to offer a unitary methodology for robust control of piezoelectric smart structures. The methodology is validated by laboratory tests. Only few similar works are reported in the literature of the field.

The paper is structured as follows. In Section 2, the mathematical model of the smart structure is presented. Based on the mathematical model, Section 3 details three levels of H_∞ control synthesis. As comparison term for robust H_∞ control synthesis, Section 4 resumes a simple and efficient procedure of LQG/LTR control design. In Section 5, we present some experimental results on an elementary smart structure, a cantilever plate. The paper ends with some concluding remarks.

2 MATHEMATICAL MODELING OF THE SMART STRUCTURE

A plate is defined as a structure whose thickness is small as compared with the other two dimensions. The smart plate is modeled as a composite laminated plate based on the Kirchoff hypothesis. The actuators are modeled in the framework of the linear piezoelectric theory. The system is discretized by the Rayleigh-Ritz method; a pseudo-analytical model is thus obtained. An approximate mathematical model can be also obtained by using the finite element method (FEM). In practice, finite models are considered by limiting the number of degrees of freedom to one deemed representative during the structural modeling phase, i.e. limiting the number of modes in the series expansion of the assumed modes method or through choosing a finite number of nodes in an FEM discretization. Assuming viscous damping, the structure equations of motion can then be written

$$\mathbf{M}\ddot{\mathbf{q}} + \mathbf{C}\dot{\mathbf{q}} + \mathbf{K}\mathbf{q} = \mathbf{B}^{pz}\mathbf{u} + \mathbf{f} \qquad (1)$$

Ursu I., Iorga L., Toader A. and Tecuceanu G..
ACTIVE ROBUST CONTROL OF A SMART PLATE.
DOI: 10.5220/0003649504900499
In *Proceedings of the 8th International Conference on Informatics in Control, Automation and Robotics* (ICM-2011), pages 490-499
ISBN: 978-989-8425-74-4

where **M**, **C**, **K** are the mass, structural damping and stiffness matrices, respectively, while **q**, **u** and **f** are the generalized coordinates, control inputs and generalized loads. The matrix $\mathbf{B}^{pz}$ contains the piezoelectric influence coefficients. Consider now the transformation to modal coordinates

$$\mathbf{q}(t) = \mathbf{V}\boldsymbol{\eta}(t) \tag{2}$$

where **V** is the matrix of normalized eigenvectors $\mathbf{v}_i$ satisfying $\left(\mathbf{K} - \omega_i^2\mathbf{M}\right)\mathbf{v}_i = \mathbf{0}, i = 1,...,m$. Because $\mathbf{V}^T\mathbf{M}\mathbf{V} = \mathbf{I}$, the equations of motion become

$$\ddot{\boldsymbol{\eta}} + \tilde{\mathbf{C}}\dot{\boldsymbol{\eta}} + \tilde{\mathbf{K}}\boldsymbol{\eta} = \tilde{\mathbf{B}}^{pz}\mathbf{u} + \tilde{\mathbf{f}} \tag{3}$$

where $\tilde{\mathbf{C}} = \mathbf{V}^T\mathbf{C}\mathbf{V}, \tilde{\mathbf{K}} = \mathbf{V}^T\mathbf{K}\mathbf{V}, \tilde{\mathbf{B}}^{pz} = \mathbf{V}^T\mathbf{B}^{pz}$. The modal damping and stiffness matrices $\tilde{\mathbf{C}}$ and $\tilde{\mathbf{K}}$ are diagonal but, in general, the modal equations of motion (3) remain coupled through the components of matrix $\tilde{\mathbf{B}}^{pz}$.

For the control synthesis, the system must be written as a system of first order ordinary differential equations. Denote by **x** the state vector $\mathbf{x} = [\boldsymbol{\eta} \quad \dot{\boldsymbol{\eta}}]^T$. Then from equation (3) we obtain the *state equations*:

$$\dot{\mathbf{x}} = \mathbf{A}\mathbf{x} + \mathbf{B}_1\tilde{\mathbf{f}} + \mathbf{B}_2\mathbf{u} \tag{4}$$

where the system matrices are:

$$\mathbf{A} = \begin{bmatrix} \mathbf{0} & \mathbf{I} \\ -\tilde{\mathbf{K}} & -\tilde{\mathbf{C}} \end{bmatrix}, \mathbf{B}_1 = \begin{bmatrix} \mathbf{0} \\ \mathbf{I} \end{bmatrix}, \mathbf{B}_2 = \begin{bmatrix} \mathbf{0} \\ \tilde{\mathbf{B}}^{pz} \end{bmatrix} \tag{5}$$

The system output equations are grouped in *regulated* variables, which characterize the objectives to be attained through control and *measured* variables which represent directly the sensor output. The measurement equation is

$$\mathbf{y} = \mathbf{C}_2\mathbf{x} + \tilde{\mathbf{D}}_{21}\boldsymbol{\mu} + \mathbf{D}_{22}\mathbf{u} \tag{6}$$

where **y** is the measured sensor output vector, $\boldsymbol{\mu}$ is the vector of measurement (sensor) noise, and the specific form of the measurement matrices $\mathbf{C}_2$, $\mathbf{D}_{21}$ and $\mathbf{D}_{22}$ depends on the type of measurement considered. Optical displacement measurements, acceleration measurements, strain measurements – either by using strain gages, or piezoelectric bonded patches – are reported in the literature. When measuring quantities such as displacements or strains, the exogenous perturbation $\tilde{\mathbf{f}}$ and the control inputs **u** have no direct effect on the measured outputs. Then

$$\mathbf{D}_{22} = \mathbf{0} \tag{7}$$

In its most general form, the output equation for the regulated variables **z** can be hereby written

$$\mathbf{z} = \mathbf{C}_1\mathbf{x} + \mathbf{D}_{11}\tilde{\mathbf{f}} + \mathbf{D}_{12}\mathbf{u} \tag{8}$$

thus relating the regulated output to the system state as well as exogenous perturbations and control inputs. The choice most often encountered in the literature of the field for the regulated outputs is to use directly the sensor measurements weighted in the frequency domain. Alternatively, other quantities representative to the system response can be employed. For example, the amplitudes of the modal coordinates and velocities; in this case, the regulated variables vector is

$$\mathbf{z} = \left[\eta_1,...,\eta_{m_1},\dot{\eta}_1,...,\dot{\eta}_{m_2},u_1,...,u_{N_{act}}\right]^{\mathrm{T}} \tag{9}$$

For this case, the output reflection of the actuator inputs is achieved through the matrix $\mathbf{D}_{12}$ whose first rows are null since the control input **u** has no direct effect on the modal coordinates and velocities. Since the regulated output contains modal coordinates and velocities and the piezoelectric actuator inputs, the perturbations $\tilde{\mathbf{f}}$ have no direct effect on the regulated variables – therefore the matrix $\mathbf{D}_{11}$ will simply be a null matrix. Thus

$$\mathbf{D}_{11} = [\mathbf{0}], \mathbf{D}_{12} = \begin{bmatrix} \mathbf{0} \\ \mathbf{I} \end{bmatrix} \tag{10}$$

3 H_∞ CONTROL SYNTHESIS

3.1 The Case of Static Weights

We consider the following basic equations of the smart structure system as processed from the equations (4), (6), (8), by taking into account the logistics defining the experimental specimen presented in Figures 1, 2

$$\begin{gathered} \dot{\mathbf{x}} = \mathbf{A}\mathbf{x} + \mathbf{B}_1\mathbf{u}_1 + \mathbf{B}_2u_2 \\ y = \mathbf{C}_2\mathbf{x} + \mathbf{D}_{21}\mathbf{u}_1 + D_{22}u_2 \\ \mathbf{z} = \mathbf{C}_1\mathbf{x} + \mathbf{D}_{11}\mathbf{u}_1 + \mathbf{D}_{12}u_2 \\ \mathbf{x} \in \mathbf{R}^n, \mathbf{u}_1 \in \mathbf{R}^2, \mathbf{u}_1 := \begin{bmatrix} \tilde{f} \\ \mu \end{bmatrix}, y \in \mathbf{R}, \mathbf{z} \in \mathbf{R}^{n+1} \\ \mathbf{C}_2 \in \mathbf{R}^{1\times n}, \mathbf{C}_1 \in \mathbf{R}^{(n\times 1)\times n} \\ \mathbf{C}_1 = \begin{bmatrix} \rho_{\mathbf{x}}\mathbf{diag}(\mathbf{C}_2) \\ \mathbf{0}^{1\times n} \end{bmatrix}, D_{12} = \begin{bmatrix} \mathbf{0}^{n\times 1} \\ \rho_{\mathbf{u}_2} \end{bmatrix} \end{gathered} \tag{11}$$

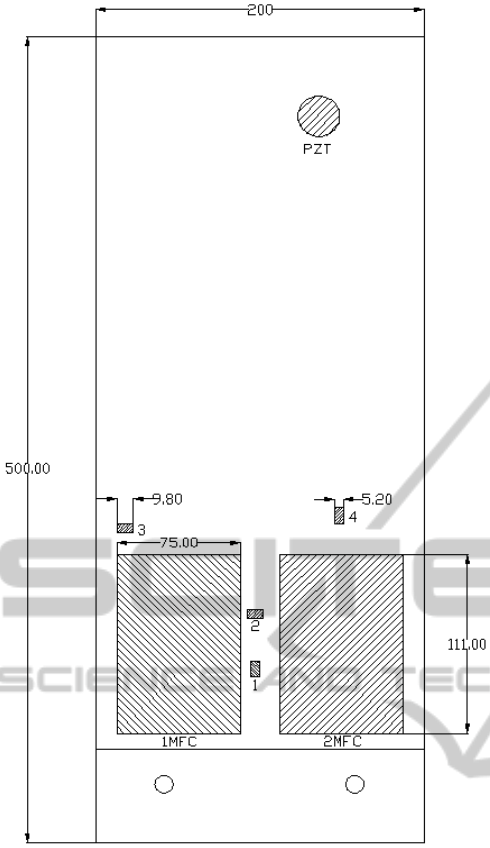

Figure 1: Sketch of the basic smart structure considered for this study – the cantilevered aluminum plate with bonded MFC actuators. Legend: 1MFC – the Macro Fiber Composite (MFC) active control actuator; 2MFC – MFC actuator for disturbance generation; 1, 1, 2, 4 – strain gages.

The realization of the transfer matrix $\mathbf{G}(\mathbf{s})$ is transcribed in the usual form

$$\mathbf{G}(\mathbf{s}) = \left[\begin{array}{c|cc} \mathbf{A} & \mathbf{B}_1 & \mathbf{B}_2 \\ \hline \mathbf{C}_1 & \mathbf{D}_{11} & \mathbf{D}_{12} \\ \mathbf{C}_2 & \mathbf{D}_{21} & \mathbf{D}_{22} \end{array}\right] := \left[\begin{array}{c|c} \mathbf{A} & \mathbf{B} \\ \hline \mathbf{C} & \mathbf{D} \end{array}\right] = \mathbf{C}(\mathbf{sI}-\mathbf{A})^{-1}\mathbf{B}+\mathbf{D} \quad (12)$$

These equations characterize a SISO (Single-Input-Single-Output) system, for which an H_∞ optimal control problem is posed: find a controller $\mathbf{K}(\mathbf{s})$ that will minimize the peak value of the frequency response of $\mathbf{T}_{zu_1}(s)$, the matrix-valued closed-loop transfer function from the system input to its output (see Fig. 4). In other words, the question is to find a controller $\mathbf{K}(\mathbf{s})$

$$\mathbf{K}(\mathbf{s}) = \left[\begin{array}{c|c} \mathbf{A_c} & \mathbf{B_c} \\ \hline \mathbf{C_c}\,(:=\mathbf{K}_\infty) & \mathbf{D_c} \end{array}\right] \begin{array}{l} \dot{\mathbf{x}}_c = \mathbf{A}_c\mathbf{x}_c + \mathbf{B}_c y \\ \mathrm{u}_2 = \mathbf{C}_c\mathbf{x}_c + D_c y \end{array} \quad (13)$$

that internally stabilizes the closed-loop system and that, given $\gamma > 0$, satisfies the condition

$$\left\|\mathbf{T}_{zu_1}\right\|_\infty := \sup_{\omega\in R} \bar{\sigma}\left[\mathbf{T}_{zu_1}(j\omega)\right] < \gamma \quad (14)$$

Figure 2: Photo of the cantilever aluminum plate specimen performed for active control laws validation.

A justification for the optimal H_∞ control resides in the *minimax* nature of the problem, with the argument that minimizing the "peak" of the transfer $u_1 \to z$ necessarily renders the magnitude of $\mathbf{T}_{\mathbf{zu_1}}$ small at all frequencies. In other words, minimizing the H_∞-norm of a transfer function is equivalent to minimizing the energy in the output signal due to the inputs with the worst possible frequency distribution. This improvement of the "worst-case scenario" has a direct correspondent in the active vibration control problem and seems particularly attractive for light structures with embedded piezoelectric actuators.

Before H_∞ control synthesis can be employed, it is necessary to verify that the open-loop plant satisfies several assumptions (Zhou *et al.*, 1996). Specific desired loop gain are (Postletwhite and Skogestad, 1993): a) for perturbation rejection make $\underline{\sigma}(\mathbf{KG})$ large and b) for noise attenuation make $\bar{\sigma}(\mathbf{KG})$ small (Figure 3). The specific low frequency ω_l and high frequency ω_h depend on the specific applications.

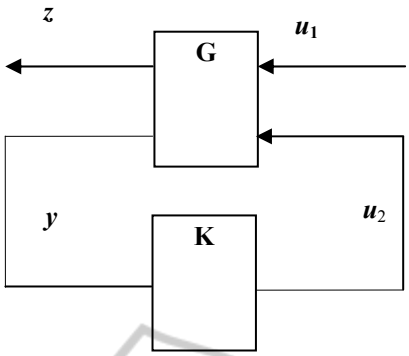

Figure 3: The H_∞ control paradigm.

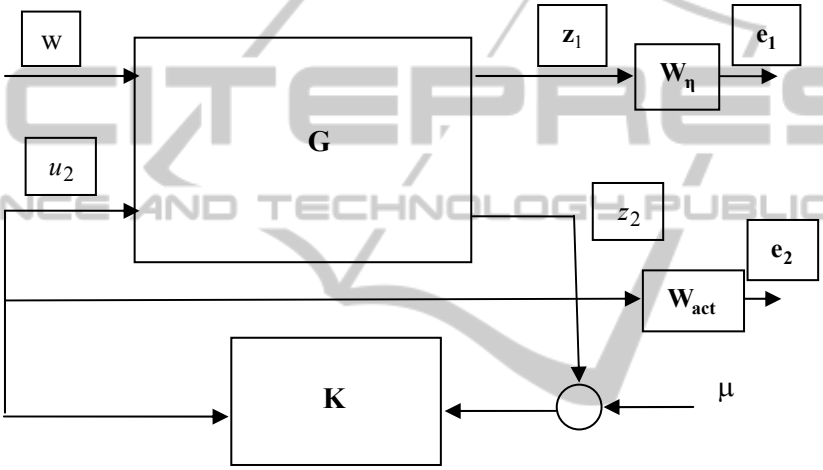

Figure 4: Block diagram of the augmented system. Dynamic weights.

We note that the observer-based H_∞ controller (12) is a *dynamic* one, even though it is based on *static weights*, see the matrices $\mathbf{C_1}, \mathbf{D_{12}}, \mathbf{D_{21}}$.

3.2 Augmented System: Dynamic Weighting Functions

The system inputs and outputs can be modified in order to specify certain performance objectives to be met by the closed-loop system, and to account for the relative magnitude of the signals (Zhou *et al.*, 1996). Consider the system of equations (11) with weighted regulated outputs as shown in Figure 6, where the loop is closed by the controller $\mathbf{K}$, yet to be determined. We denote by $\mathbf{W_\eta}$ the diagonal transfer matrix of first-order low pass filter, weighting the modal coordinates in the regulated outputs vector and by $\mathbf{W_{act}}$ the transfer matrix of second order band-stop filters, or first-order high-pass filters, weighting on the piezoelectric control voltages

$$W_{\eta i} = \frac{k_{\eta i}}{\frac{1}{k_i \omega_i} s + 1}, i = 1, \ldots, n,$$

$$W_{act} = k_{act} \frac{\left(\frac{1}{\omega_{act_2}} s + 1\right)\left(\frac{1}{\omega_{act_3}} s + 1\right)}{\left(\frac{1}{\omega_{act_1}} s + 1\right)\left(\frac{1}{\omega_{act_4}} s + 1\right)} \tag{15}$$

$$\mathbf{W_\eta} = \left[\begin{array}{c|c} \mathbf{A_\eta} & \mathbf{B_\eta} \\ \hline \mathbf{C_\eta} & \mathbf{D_\eta} \end{array}\right], \mathbf{W_{act}} = \left[\begin{array}{c|c} \mathbf{A_{act}} & \mathbf{B_{act}} \\ \hline \mathbf{C_{act}} & \mathbf{D_{act}} \end{array}\right]$$

The idea is to place greater emphasis on suppressing the response due to low-frequency excitation while avoiding a response to small high-frequency components which will excite faster modes. Further on, the piezo actuator signals are subject to identical weighting functions $\mathbf{W_{act}}$ chosen such that at

undesired very low and at high frequencies, herein, the weight magnitude is increased, thus reducing the controller response, while in the target bandwidth it is decreased. Thus, partitioning the matrix $\mathbf{C_1} := \left[\mathbf{C_{11}^T} \quad \mathbf{0}\right]^T$, we can write the augmented system (Figure 4)

$$\dot{\mathbf{x}}_\eta = \mathbf{A}_\eta \mathbf{x}_\eta + \mathbf{B}_\eta \mathbf{z}_1 = \mathbf{A}_\eta \mathbf{x}_n + \mathbf{B}_n \mathbf{C}_{11} \mathbf{x}, \dot{\mathbf{x}}_{act} =$$
$$= \mathbf{A}_{act} \mathbf{x}_{act} + \mathbf{B}_{act} \mathbf{z}_2 = \mathbf{A}_{act} \mathbf{x}_{act} + \mathbf{B}_{act} u_2$$

$$\mathbf{e}_1 = \mathbf{C}_\eta \mathbf{x}_\eta + \mathbf{D}_\eta \mathbf{z}_1 = \mathbf{C}_\eta \mathbf{x}_\eta + \mathbf{D}_\eta \mathbf{C}_{11} \mathbf{x}, \mathbf{e}_2 =$$
$$= \mathbf{C}_{act} \mathbf{x}_{act} + \mathbf{D}_{act} u_2, y = \mathbf{C}_2 \mathbf{x} + \mathbf{D}_{21} \mathbf{w}$$

$$\begin{bmatrix} \dot{\mathbf{x}} \\ \dot{\mathbf{x}}_\eta \\ \dot{\mathbf{x}}_{act} \end{bmatrix} = \begin{bmatrix} \mathbf{A} & \mathbf{0} & \mathbf{0} \\ \mathbf{B}_\eta \mathbf{C}_{11} & \mathbf{A}_\eta & \mathbf{0} \\ \mathbf{0} & \mathbf{0} & \mathbf{0} \end{bmatrix} \begin{bmatrix} \mathbf{x} \\ \mathbf{x}_\eta \\ \mathbf{x}_{act} \end{bmatrix} + \begin{bmatrix} \mathbf{B}_1 \\ \mathbf{0} \\ \mathbf{0} \end{bmatrix} \mathbf{u}_1 + \begin{bmatrix} \mathbf{B}_2 \\ \mathbf{0} \\ \mathbf{B}_{act} \end{bmatrix} u_2 \quad (16)$$

$$\begin{bmatrix} \mathbf{e}_1 \\ \mathbf{e}_2 \\ y \end{bmatrix} = \begin{bmatrix} \mathbf{D}_\eta \mathbf{C}_{11} & \mathbf{C}_\eta & \mathbf{0} \\ \mathbf{0} & \mathbf{0} & \mathbf{C}_{act} \\ \mathbf{C}_2 & \mathbf{0} & \mathbf{0} \end{bmatrix} \begin{bmatrix} \mathbf{x} \\ \mathbf{x}_\eta \\ \mathbf{x}_{act} \end{bmatrix} + \begin{bmatrix} \mathbf{0} \\ \mathbf{0} \\ \mathbf{D}_{21} \end{bmatrix} \mathbf{u}_1 + \begin{bmatrix} \mathbf{0} \\ \mathbf{D}_{act} \\ \mathbf{0} \end{bmatrix} u_2$$

4 LQG/LTR CONTROL SYNTHESIS

Consider Single-Input-Single-output (SISO) system. The LQG (Linear Quadratic Gaussian) (Kalman, 1960) control synthesis concerns the system

$$\dot{\mathbf{x}} = \mathbf{A}\mathbf{x} + \tilde{\mathbf{B}}_1 \tilde{\mathbf{f}} + \mathbf{B}_2 u, \ \mathbf{z} = \mathbf{C}_1 \mathbf{x}, \ y = \mathbf{C}_2 \mathbf{x} + \tilde{D}_{21} \mu \quad (17)$$

and a stochastic framework which assumes the exogenous signals $\tilde{\mathbf{f}}$ and μ display the characteristics of white noise signals. The goal is to find a control $\mathbf{u}$ such that the system is stabilized and the control minimizes the cost function

$$J_{LQG} = \lim_{T \to \infty} \frac{1}{T} E\left\{\int_0^T \begin{bmatrix} \mathbf{x}(t)^T & u(t) \end{bmatrix} \begin{bmatrix} \mathbf{Q} & \mathbf{0} \\ \mathbf{0} & R \end{bmatrix} \begin{bmatrix} \mathbf{x}(t) \\ u(t) \end{bmatrix} dt\right\} \quad (18)$$
$$\mathbf{Q} = \mathbf{C}_1^T \mathbf{Q}_J \mathbf{C}_1, \ R = \rho$$

where $\mathbf{Q}_J$ and ρ are weights (ρ is herein scalar). The solution is given by the classical Kalman synthesis. The state estimator has the form

$$\dot{\hat{\mathbf{x}}} = \mathbf{A}\hat{\mathbf{x}} + \mathbf{B}_2 \mathbf{u} + \mathbf{K}_f \left(y - \mathbf{C}_2 \hat{\mathbf{x}}\right) \quad (19)$$

The LQG control synthesis concerns the solving of the decoupled algebraic Riccati equations

$$\begin{aligned} \mathbf{A}^T \mathbf{P} + \mathbf{P}\mathbf{A} - \mathbf{P}\mathbf{B}_2 R^{-1} \mathbf{B}_2^T \mathbf{P} + \mathbf{C}_1^T \mathbf{Q}_J \mathbf{C}_1 = \mathbf{0} \\ \mathbf{A}\mathbf{S} + \mathbf{S}\mathbf{A}^T - \mathbf{S}\mathbf{C}_2^T \mathbf{Q}_\mu^{-1} \mathbf{C}_2 \mathbf{S} + \tilde{\mathbf{B}}_1 \mathbf{Q}_{\tilde{f}} \tilde{\mathbf{B}}_1^T = 0 \end{aligned} \quad (20)$$

where $\mathbf{Q}_{\tilde{\mathbf{f}}}$ and Q_μ are the matrices describing the noise characteristics. The control u, the controller gain, $\mathbf{K_c}$, the filter gain, $\mathbf{K_f}$, and the filter matrix, respectively, are defined by,

$$\begin{aligned} u(t) = -\mathbf{K}_c \hat{\mathbf{x}}(t) \\ \mathbf{K}_c = \mathbf{R}^{-1} \mathbf{B}_2^T \mathbf{P}, \ \mathbf{K}_f = \mathbf{S}\mathbf{C}_2^T \mathbf{Q}_{\tilde{f}}^{-1} \\ \mathbf{A}_0 = \mathbf{A} - \mathbf{B}_2 \mathbf{K}_c - \mathbf{K}_f \mathbf{C}_2 \end{aligned} \quad (21)$$

Using the state-estimator and the control law, the closed loop system becomes

$$\begin{aligned} \dot{\mathbf{x}}(t) = \mathbf{A}\mathbf{x}(t) + \mathbf{B}_1 \tilde{\mathbf{f}}(t) - \mathbf{B}_2 \mathbf{K}_c \hat{\mathbf{x}}(t) \\ \dot{\hat{\mathbf{x}}}(t) = \mathbf{K}_f \mathbf{C}_2 \mathbf{x}(t) + \mathbf{K}_f \tilde{D}_{21} \mu(t) + \mathbf{A}_0 \hat{\mathbf{x}}(t) \end{aligned} \quad (22)$$

It is well known that the Linear Quadratic Regulator (LQR) controller has good robustness properties, but these properties are usually lost when the LQR is used in conjunction with the Kalman filter (Doyle, 1978). In the following, the LQG/LTR (Loop Transfer Recovery) procedure (Stein and Athans, 1987) will be applied to recover the lost robustness of the LQR system. The filter gain synthesis will be performed such that

$$\mathbf{B_1} = \mathbf{B_2}, \tilde{D}_{12} \to 0 \quad (23)$$

and also, such that

$$\mathbf{L_{LQG}}(j\omega) \cong \mathbf{L_{LQR}}(j\omega) \quad (24)$$

in a certain range, as large as possible $\omega \in [0, \omega_{max}]$, where $(j\omega = s)$

$$\begin{aligned} \mathbf{L_{LQG}}(\mathbf{s}) = -\mathbf{K}_c (\mathbf{sI} - \mathbf{A} - \mathbf{K}_f \mathbf{C}_2 - \mathbf{B}_2 \mathbf{K}_c)^{-1} \\ \mathbf{K}_f \mathbf{C}_2 (\mathbf{sI} - \mathbf{A})^{-1} \mathbf{B}_2 \\ \mathbf{L_{LQR}}(\mathbf{s}) = -\mathbf{K}_c (\mathbf{sI} - \mathbf{A})^{-1} \mathbf{B}_2 \end{aligned} \quad (25)$$

Thus, the filter gain $\mathbf{K_f}$ will be tuned so that the closed-loop LQG/LTR system (having the open loop matrix $\mathbf{L_{LQG}}$) recovers internal stability and some of the robustness properties (gain and phase margins)

of the LQR design (with open loop matrix $\mathbf{L_{LQR}}$). Moreover, standard statements similar to those already enunciated can be added: a) for perturbation rejection $\underline{\sigma}(\mathbf{L_{LQG}})$ is to be designed large and b) for noise attenuation $\bar{\sigma}(\mathbf{L_{LQG}})$ is to be designed small.

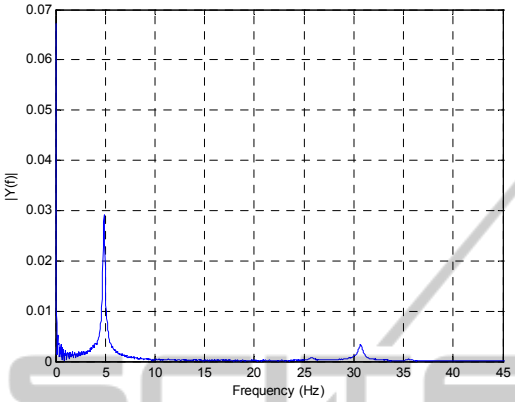

Figure 5: Results on cantilever plate process identification.

5 EXPERIMENTAL RESULTS ON AN ELEMENTARY SMART STRUCTURE

To test the proposed smart structures control strategies, a 200×500×1.25 mm cantilever aluminum plate (Figures 1, 2) is considered. The test rig contains 1) the cantilever aluminum plate on which the strain gages (SGD-5/350-LY11, Omega Engineering) and MFC (M8557P1MFC, Smart Materials) actuators are bonded, 2) the signal conditioners (OM5-WBS-3-C, Omega Engineering) for converting strain gages bridge signals to high level and for bridge supply, 3) the high voltage amplifiers (PA05039,-500 V÷ +1500V) for the MFC actuators supply, 4) a PC on which the control laws are implemented and 5) an acquisition card (NI PCIe-6259) used for processing the signals from conditioners and for applying to the MFC actuator the control signal, amplified by the high voltage amplifiers.

The values of the matrices $\mathbf{A}, \tilde{\mathbf{B}}_1, \mathbf{B}_2, \mathbf{C}_2$ were obtained by ANSYS analysis combined with analytic considerations based on the setup of the measured and regulated outputs. We note here that only one of the strain gages bonded on specimen was operational during the tests thus limiting the experiments to a single-output case. The first five natural frequencies of the plate identified from the FE model are 5.66 Hz, 25.23 Hz, 33.95 Hz, 81.03 Hz, 95.05 Hz. Only a small modal damping factor of 1% of the critical damping was applied to the model. The experimental frequencies identified with the setup described are 5 Hz, 26 Hz, 31 Hz, 157 Hz. Figure 5 shows the results of a simple process identification procedure based on impulse type perturbation. There is an acceptable match of the first three frequencies between the model and the measured ones. However, this does not apply for the higher modes, with only the mode at 157 Hz being detected by the strain gages. Consequently, only first three modes will be taken into account in the matrix $\mathbf{C}_1$. Figure 6 presents all the system matrices defined in (12), (13) both with the "static" weights. The consistency of the first three modes in process is attested by Figure 7. The frequency responses of the weighting filters (16) are shown in Figure 8. In choosing the dynamic weights, it is to mention the continuity with the static weights

$$k_{\eta_1} = -322,\ k_{\eta_2} = -39.3,\ k_{\eta_3} = -1.0881$$

$$\omega_1 = 35.6091 \text{ rad/s}$$

$$\omega_2 = 158.5449 \text{ rad/s}\ \ k_1 = k_2 = k_3 = 2$$

$$\omega_3 = 213.3373 \text{ rad/s}$$

$$\omega_{a_1} = 18.85 \text{ rad/s},\ \omega_{a_4} = 1885 \text{ rad/s}$$

$$\omega_{a_2} = 25.13 \text{ rad/s},\ k_{act} = 0.5,\ \omega_{a_3} = 219.9 \text{ rad/s}$$

The steps of H_∞ control synthesis, described in Sections 3.1 and 3.2, have been validated by numerical simulations and experiments (see Figures 9, 10). A notable vibration attenuation of 17.4 dB is experimentally reached (Figure 10). For the sake of comparison, we cite the result 15.6 dB in (Yaman *et al.*, 2002). The simulation result predicts a somewhat better performance, with a value of 26 dB for the attenuation (Figure 9). The attenuation values in the case of dynamic weights are similar. The better attenuation predicted by the model is explained primarily by the very small value of damping introduced in the model, very likely significantly smaller than the true damping value. This essentially leads to an over-prediction of the vibration amplitudes in the simulations. Additionally, the actuator efficiency in the model is considered to be ideal. A perfect actuator bonding to the plate base structure was assumed, without any modeling of the adhesive bond-line effects. Also, the actuator electro-mechanic behavior was assumed to be linear, without accounting for any hysteretic or other nonlinear effects. Finally, we note that the controller is derived for the numerical model, and

thus a certain reduction in performance is to be expected when applied to the real structure.

We emphasize now the reason for justifying the use of an H_∞ augmented system, instead of nominal one. When exciting the structure at 157 Hz, close to the fourth natural frequency, control spillover is noticeable. The fourth mode is not accounted for into the structural model during the controller synthesis phase and thus susceptible to spillover. Figure 11 exemplifies this phenomenon for the case of closed loop control with static-weights. However, the controller response can be significantly reduced through weighting the regulated output variable, as shown in Figure 12. The application of the robust LQG/LTR control law is exemplified in Figure 13.

6 CONCLUDING REMARKS

This paper shows how to handle the apparatus of applied control for the problem of active vibration control design in smart structures. Both the theoretical background and the logistics defining the experimental specimen are presented. Two different approaches for the synthesis of robust control are detailed – robust H_∞ control and LQG/LTR control, as comparison term. It is worth noting the theoretical apparatus is confirmed by laboratory tests. Dynamic weights were successfully used as a method to prevent H_∞ control saturation. Also, the experimental results show a comparable trend with others reported in the literature.

$$A = \begin{bmatrix} \boldsymbol{0}_{5\times5} & \boldsymbol{I}_{5\times5} \\ \begin{matrix} -1270 & 0 & 0 & 0 & 0 \\ 0 & -25140 & 0 & 0 & 0 \\ 0 & 0 & -45510 & 0 & 0 \\ 0 & 0 & 0 & -259270 & 0 \\ 0 & 0 & 0 & 0 & -356680 \end{matrix} & \begin{matrix} -0.7122 & 0 & 0 & 0 \\ 0 & -3.1709 & 0 & 0 \\ 0 & 0 & -4.2667 & 0 \\ 0 & 0 & 0 & -10.1837 \\ 0 & 0 & 0 & 0 \end{matrix} \\ & \begin{matrix} 0 \\ 0 \\ 0 \\ 0 \\ -11.9445 \end{matrix} \end{bmatrix}$$

$$\mathbf{B}_1 = \begin{bmatrix} \mathbf{0}_{5\times1} & \mathbf{0}_{5\times1} \\ -0.0012 & 0 \\ -0.0012 & 0 \\ -0.0029 & 0 \\ -0.0015 & 0 \\ 0.0011 & 0 \end{bmatrix}, \mathbf{B}_2 = \begin{bmatrix} \mathbf{0}_{5\times1} \\ -0.0012 \\ 0.0012 \\ 0.0030 \\ 0.0016 \\ 0.001 \end{bmatrix}$$

$$\mathbf{C}_2 = \begin{bmatrix} -0.0322 & -0.0039 & -0.1088 & -0.00878 & -0.0878 & \mathbf{0}_{1\times5} \end{bmatrix}$$

$$\mathbf{D}_{21} = 10^{-8} \times \begin{bmatrix} 0 & 1 \end{bmatrix}, \mathbf{C}_1 = 10^4 \times \begin{bmatrix} \mathrm{diag}\left(C_2(1), C_2(2), C_2(3)\right) & 0^{3\times8} \\ 0^{1\times8} & \end{bmatrix} \times$$

$$\rho_{u_2} = 0.5$$

$$+ A_c = \begin{bmatrix} -56.9 & -7 & -195.2 & -15.5 & -157.366 & 1 & 0 & 0 & 0 & 0 \\ -10.3 & -1.2 & -34.3 & -2.7 & -28.041 & 0 & 1 & 0 & 0 & 0 \\ -38.7 & -4.7 & -129.4 & -10.4 & -105.6 & 0 & 0 & 1 & 0 & 0 \\ -1.8 & -0.2 & -6.2 & -0.4 & -5 & 0 & 0 & 0 & 1 & 0 \\ -2.4 & -0.3 & -8.3 & -0.6 & -6.7 & 0 & 0 & 0 & 0 & 1 \\ 4597.6 & -347.9 & -10852.1 & -828.0 & 8366.7 & -27.9 & 0 & -12.6 & 0 & 0 \\ 2482.7 & 25475.9 & -8744.2 & -752.0 & -7599 & 29.2 & -3.2 & 13.5 & 0 & 0 \\ -4642.9 & -483.4 & -60144.8 & -1065.5 & -10766.7 & -69.7 & 0.1 & -36.5 & 0 & 0 \\ 1316.5 & 115.4 & 3886.9 & -259015.8 & 2562.6 & 36.8 & 0 & 17 & -10.1 & 0 \\ -792.5 & -126.1 & -3008.4 & -280.2 & -359508.0 & 23.8 & -0.042 & 11.0 & 0 & -11.9 \end{bmatrix}$$

$$\mathbf{B}_c = 10^8 \times \begin{bmatrix} -0.0362 & -0.0064 & -0.0243 & -0.0012 & -0.0015 & -1.9225 & -1.7461 & -2.474 & 0.5889 & -0.6506 \end{bmatrix}^T$$

$$\mathbf{C}_c = \begin{bmatrix} 119.426 & 0.2532 & 231.2168 & 0 & 0 & 11.6708 & -0.0207 & 5.3994 & 0 & 0 \end{bmatrix}, \mathbf{D_c = 0}$$

Figure 6: The cantilever plate matrices. The system matrices defined in (12), (13) and the "static" weights.

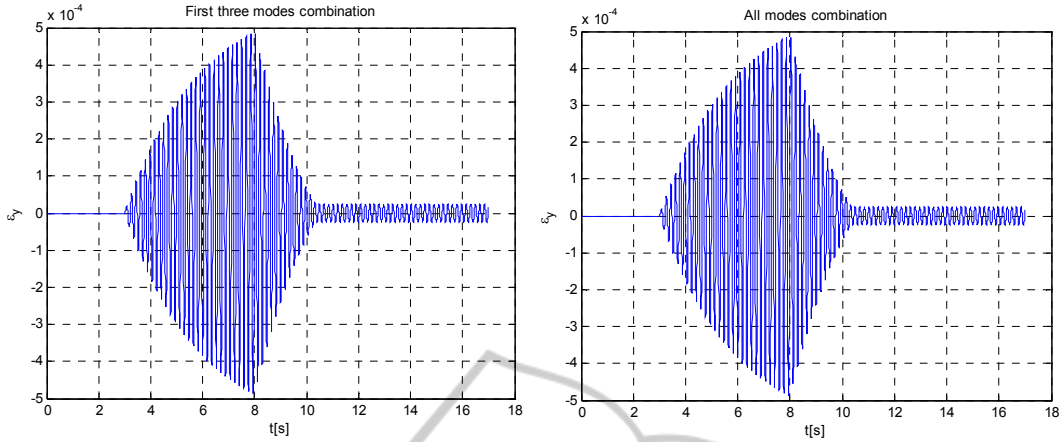

Figure 7: The consistency of the basic first three modes, static weights, $\tilde{f} = 400\sin 2\pi \times 5.66t$ V.

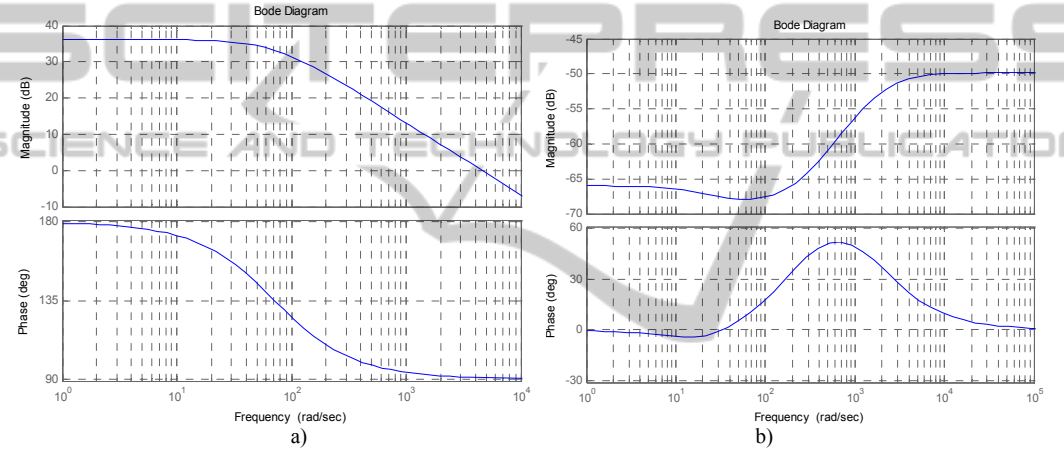

Figure 8: Weighting functions: a) $\mathbf{W_\eta}$, first mode; b) $\mathbf{W_{act}}$.

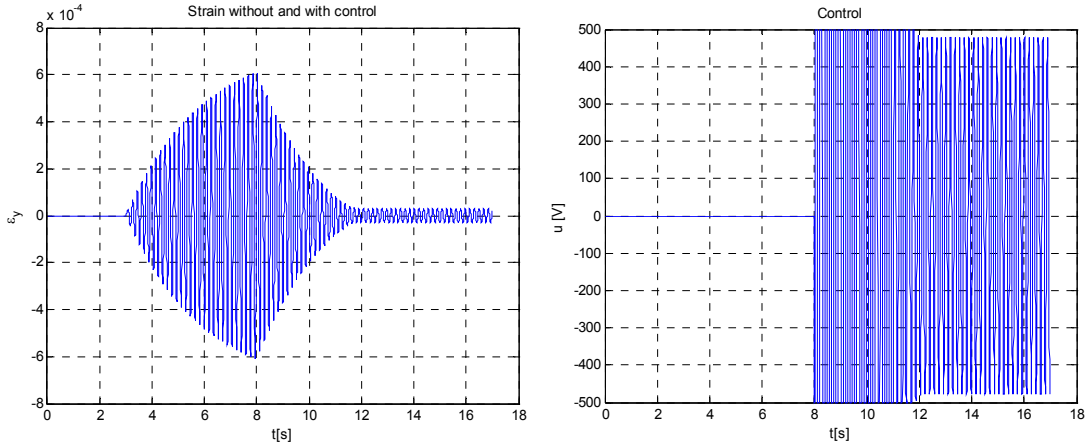

Figure 9: H_∞, static weights, numerical simulation, $\tilde{f} = 500\sin 2\pi \times 5.66t$ V.

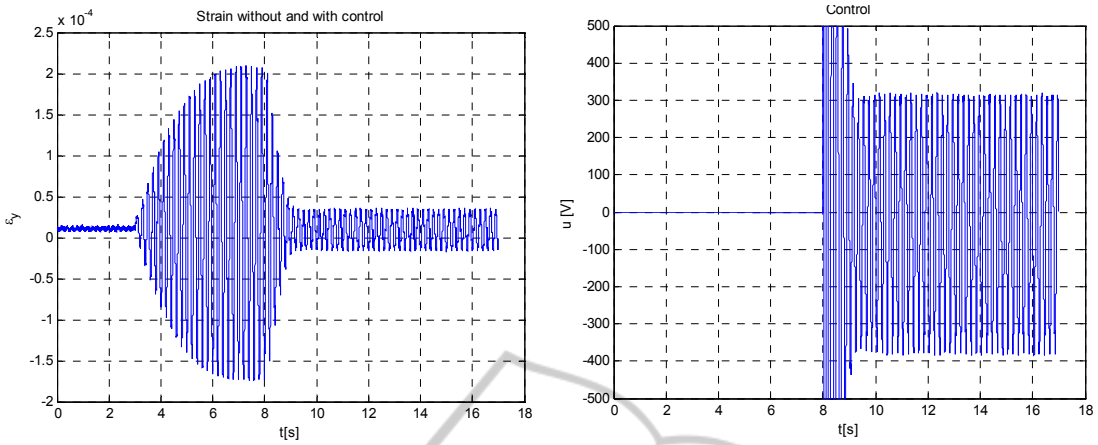

Figure 10: H_∞, static weights, experimental record, $\tilde{f} = 500\sin 2\pi \times 5t$ V.

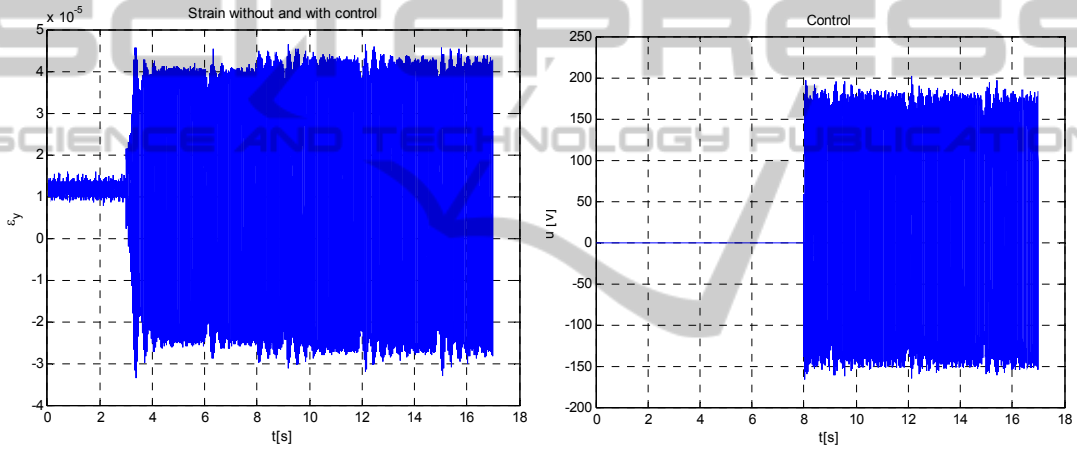

Figure 11: H_∞, static weights, experimental record, $\tilde{f} = 500\sin 2\pi \times 157t$ V.

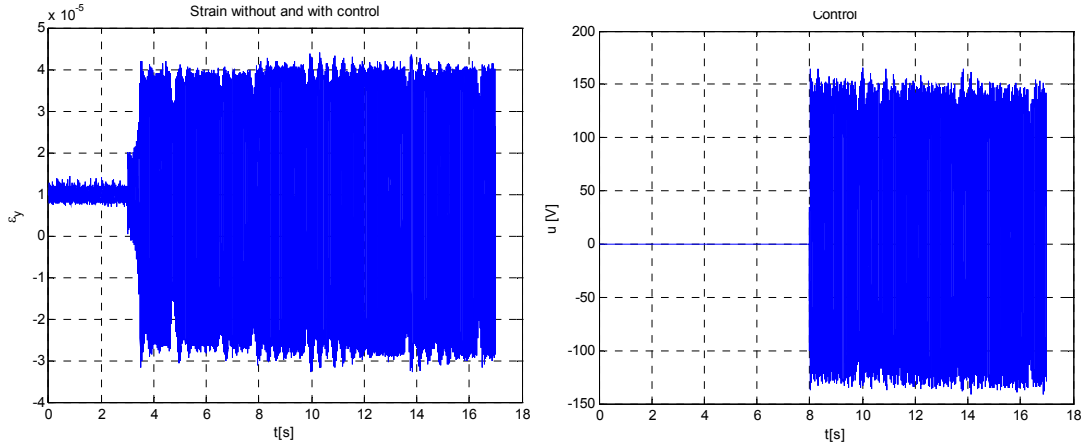

Figure 12: H_∞, dynamic weights, experimental record, $\tilde{f} = 500\sin 2\pi \times 157t$ V.

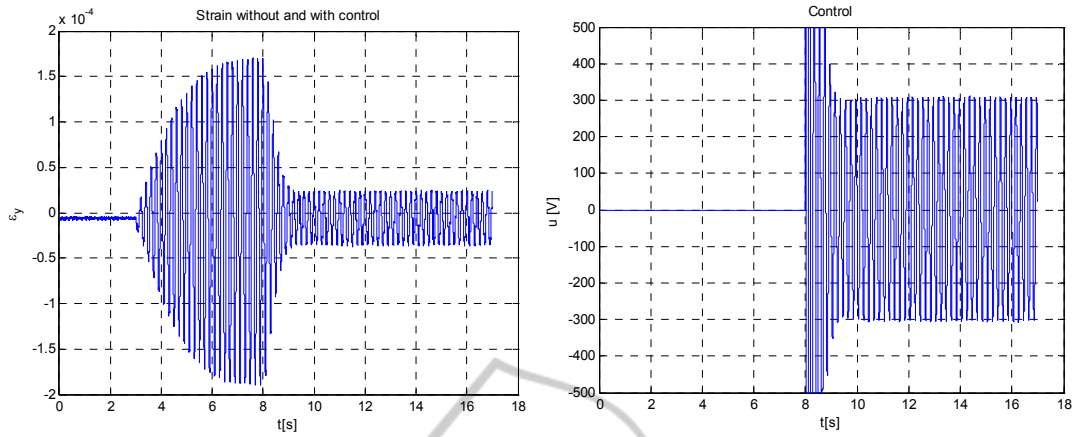

Figure 13: LQG/LTR, experimental record, $\tilde{f} = 400\sin 2\pi \times 5t$ V .

ACKNOWLEDGEMENTS

The authors from INCAS gratefully aknowledge the financial support of the National Authority for Scientific Research ANCS-UEFISCSU, through PN-II Research Project code ID 1391/2008.

REFERENCES

Doyle, J. C. (1978), Guaranteed margins for LQG regulators, *IEEE Transaction on Automatic Control*, AC-23, 4, pp. 756-757.

Iorga, L., H. Baruh, I. Ursu (2008), A review of H_∞ robust control of piezoelectric smart structures, *Transactions of the ASME*, *Applied Mechanics Reviews*, 61, 4, July, pp. 17-31.

Iorga, L., H. Baruh, I. Ursu (2009), H_∞ control with μ-analysis of a piezoelectric actuated plate, *Journal of Control and Vibration*, 15, 8, pp. 1143-1171, SAGE Publications.

Joshi, S. M., A. G. Kelkar (1998), Inner loop control for supersonic aircraft in the presence of aeroelastic modes, *IEEE Trans. on Control Systems Technology*, 6, 6, 730-739.

Kalman, R. E. (1960), Contributions to the theory of optimal control, *Bol. Soc. Mat. Mexicana*, 5, pp. 102–109.

Kar, N. I., T. Miyakura, K. Seto (2000), Bending and torsional vibration control of a flexible plate structure using based robust control law, *IEEE Trans. on Control Systems Technology*, 8, 3, pp. 545-553.

Postlethwaite, I., S. Skogestad (1993), Robust multivariable control using H_∞ methods: Analysis, design and industrial applications, in *Essays on Control – Perspectives in the Theory and its Applications*, Birkhäuser, Boston – Basel – Berlin.

Stein, G., M. Athans (1987), The LQG/LTR procedure for multivariable feedback control design, *IEEE Transactions on Automatic Control*, AC-32, 2, pp. 105-114.

Yaman, Y., T. Caliskan, V. Nalbantoglu, E. Prasad, D. Waechter (2002), Active vibration control of a smart plate, *presented at ICAS 2002*.

Ursu, I., F. Ursu (2002), *Active and semiactive control,* Romanian Academy Publishing House (in Romanian), Bucharest.

Zhou, K., J. Doyle, K. Glover (1996), *Robust and optimal control*, Prentice Hall, Upper Saddle River, NJ.